Periodic density functional theory study of Pt(111): surface features of slabs of different thicknesses

1999 J. Phys.: Condens. Matter 11 7463

(http://iopscience.iop.org/0953-8984/11/39/304)

J. Phys.: Condens. Matter **11** (1999) 7463–7480. Printed in the UK PII: S0953-8984(99)04300-3

Periodic density functional theory study of Pt(111): surface features of slabs of different thicknesses

Anton Kokalj† and Mauro Causà‡

† Department of Physical and Organic Chemistry, J Stefan Institute, Jamova 39, SI-1000 Ljubljana, Slovenia

‡ Department of Inorganic, Physical and Materials Chemistry, University of Torino, Via P Giuria 5, I-10125 Torino, Italy

Received 14 May 1999, in final form 23 August 1999

Abstract. Bulk platinum and platinum slabs one to four (111) layers thick have been studied using the HF and DFT CO–LCAO (Hartree–Fock and density functional theory crystalline-orbital and linear-combination-of-atomic-orbitals) CRYSTAL program. The objective of this paper is to test the suitability of slabs of different thicknesses for modelling the (111) surface of platinum. The cohesive properties of the bulk (lattice constant, bulk modulus, cohesive energy) are reported and the electronic structure of the platinum bulk is discussed. The surface and relaxation energies as well as the relaxation distances of the slabs were evaluated. The electronic structure of the slabs is discussed in terms of Mulliken population analysis, the density of states, the band structure and electron-density difference maps. 'Initial-state' surface-atom core-level shifts are reported, as well as atomic dipole and quadrupole moments perpendicular to the surface.

1. Introduction

Platinum surfaces have a wide scientific and technological interest, particularly because of their catalytic properties. The oxidation of carbon monoxide and the reduction of nitric oxides over transition metals (rhodium, palladium, platinum) are key reactions for air pollution control, especially in the automotive industry, where these metals are used as the active metals in three-way catalysts [1–3]. Another field of interest is the usage of platinum in the Fischer–Tropsch synthesis [4]. A platinum surface is also important from a fundamental point of view, because it can be used in prototype systems showing chemisorption and chemical reactions at surfaces.

Over the past 15–20 years, the platinum surface has attracted great interest, experimental as well as theoretical, because of its importance in the above-mentioned scientific and technological applications. The electronic structure of the surface has been measured by means of angle-resolved photoemission experiments [5]. Low-energy electron diffraction [6–9] (LEED) as well as ion scattering spectroscopy [10–12] (ISS) experiments were used for determining the geometric surface structures. Theoretical investigations of the platinum surface have been performed using various approaches. There have been some investigations using different forms of the tight-binding method, such as the linear-muffin-tin-orbitals tight-binding [5] (LMTO-TB) or extended Hückel tight-binding method [13]. Another approach, used by Tamura and Feder [14], is the fully relativistic layer Korringa–Kohn–Rostoker (KKR) formalism, whereas Benesh *et al* [15] applied the surface-embedded Green function method. Tsai and Hass [16] applied a slightly modified version of the all-electron, full-potential pseudofunction (PSF) method. From the late 1980s on, several authors [17, 18] applied the

0953-8984/99/397463+18$30.00

semi-empirical embedded-atom method (EAM) for the determination of multilayer relaxation and the surface energy. Smith *et al* [19] and Rodríguez *et al* [20] used the semi-empirical equivalent-crystal theory (ECT) for studying the same properties. In the 1990s, Pt surface stresses have been studied by several authors. Needs *et al* [21] used the pseudopotential total-energy technique, whereas Feibelman [22] applied the linear-combination-of-atomic-orbitals (LCAO) technique.

While planning research concerning platinum catalytic phenomena using the periodic slab method with the HF and DFT CO–LCAO (Hartree–Fock and density functional theory crystalline-orbital–linear-combination-of-atomic-orbitals) approximations implemented in the CRYSTAL95 code [23], we had to ensure that we were using a model of the Pt(111) surface which is realistic enough for us to get qualitative as well as quantitative results. In order to avoid redundant calculations, a good compromise between the accuracy of the model and the computational time required for the calculations must be reached. Therefore, it is appropriate to evaluate the influence of the slab thickness on the geometry, surface energetics and electronic features of the surface layer.

This paper is organized as follows. The computational method is described in the next section. In section 3 a review of our platinum bulk calculations is given, where results on calculated cohesive (lattice constant, cohesive energy, bulk modulus) and some electronic properties (band structure, density of states, electron-density difference) will be discussed. In section 4 the calculations for various slabs are presented. The first part of the section is devoted to surface energetics and related properties (relaxation distances, relaxation energies, surface energies), whereas the second part deals with electronic properties (Mulliken population, density of states, band structure, electron-density difference, surface-atom core-level shift) of Pt(111) slabs of different thicknesses.

2. Computational details

The present work is among the first attempts to treat a transition metal surface using the periodic CO–LCAO program CRYSTAL [23]. Linear combinations of Gaussian-type orbitals were used as variational functions. Since all-electron basis sets are not practical from a computational viewpoint, the relativistic effective-core potential (RECP) was used to describe the inner shells of the Pt atoms. The RECP of Stevens *et al* [24] was adopted and the f-projection term was omitted, since our previous cluster calculations showed that the influence of the f-projection term is negligible [25]. For the Pt valence electrons, the associated basis set (designated as SBKJC) contains two very diffuse functions, and therefore it should be modified. The most diffuse sp and d functions were omitted, while in the periodic systems such functions can lead to wasting of computational resources or even cause linear dependence of the basis set. Thus instead of the original SBKJC set expressed in terms of (7s7p5d/4s4p3d), the (6s6p4d/3s3p2d) basis set was used. The basis set produced in this way is of double-zeta quality. Although the most diffuse functions were omitted, the basis set still possesses one diffuse d and one diffuse sp shell, because the presence of such diffuse shells is of major importance in metallic systems in order to ensure a uniform electron density in the interstitial regions.

The theoretical description of metallic systems is more critical than those of ionic and covalent systems, since very delocalized bands are described poorly by the LCAO approximation. However, some metal systems have been studied by this method [22, 26–31]. The self-consistent-field (SCF) convergence is very poor, especially when some symmetry is broken, as in the case of slabs. Methods dealing with an acceleration of the SCF convergence are of great importance. We found that a very simple two-point mixing of the Kohn–Sham matrices with variable coefficients, as described by Moruzzi, Janak and Williams [32] for mixing the

densities, coupled with Pulay's DIIS (direct inversion of iterative subspace) extrapolation [33], can help appreciably. The best results were accomplished by applying the two-point mixing as well as DIIS extrapolation when the energy convergence was lower than 10^{-2} au. Unrestricted calculations reduce convergence problems significantly even in the singlet case ($S = 0$). Due to the additional variational freedom, the unrestricted energy should lie, in principle, below the restricted one, but the difference is negligible as long as the system is near equilibrium geometry. Some of the important parameters in calculations using the CRYSTAL code concern the reciprocal-space integration. 72 k-points of a Monkhorst net [34] belonging to the irreducible part of the Brillouin zone were used in bulk calculations and 19 k-points were used for slab calculations. Bands were interpolated using 87 symmetrized plane waves in denser nets (Gilat nets [35]) of 413 k-points and 61 k-points for the bulk and slab, respectively. The Fermi surface was then approximated quadratically in a spherical domain around each k-point of the Gilat net.

Density functional theory was used in the present study. It is well known that the local density approximation (LDA) is particularly suited for homogeneous systems like bulk metals, but for surface studies it might be of importance to apply the generalized gradient approximation (GGA), which depends not only on electron density but also on its gradients. In the current work we have applied both approximations—namely, the Dirac–Slater [36] local spin-density exchange with the Vosko–Wilk–Nusair correlation potential [37] (LDA/VWN) and the Becke exchange potential [38] with the Perdew–Wang correlation potential [39] (BPW91). Most of the results were calculated with the LDA, since it exhibits better SCF convergence and gives results not worse than those for the GGA. Nevertheless, bulk and surface cohesive properties were calculated with the GGA as well. On the other hand, the electronic structures of the bulk and slabs were studied only by using the LDA/VWN, since different functionals produce similar electron densities [40]; that is, the functional is not terribly critical in studying properties based on electron density.

3. Platinum bulk

In order to investigate the surface properties of platinum and the processes of adsorption on it, it is desirable to study the bulk first. There are no problems in comparing our results with those obtained from the literature, because studies of the platinum bulk are available. Probably the most commonly used approach in studying the platinum bulk are different variants of the augmented-plane-wave method, also using some relativistic treatment [41–43]. Elsässer *et al* [44] treat the ground-state properties of the 5d transition metals (including platinum) using the mixed-basis pseudopotential method. Further references to theoretical investigations of platinum can be obtained elsewhere [45].

Although the HF and DFT CO–LCAO approximation implemented in the CRYSTAL code [23] is more often used for a description of ionic and covalent crystals, it seems to be good enough to describe transition metals as well. This is due to the more tightly bound nature of narrow d bands. As demonstrated by numerous tight-binding studies (using atomic orbitals) of transition metals [46], calculations using a non-plane-wave basis can be successfully applied to transition metal studies.

3.1. Cohesive properties

Since bulk calculations are very fast, it is straightforward to apply different functionals. Beside the previously mentioned LDA/VWN and BPW91 functionals, the Becke exchange potential [38] with the Lee–Yang–Parr correlation potential [47] (BLYP), and the

Perdew–Burke–Ernzerhof exchange as well as the correlation potential [48] (PBE) were used. Since the CRYSTAL code allows Hartree–Fock [49] (HF) calculation, we compare DFT results with HF ones as well.

Table 1 shows our calculated equilibrium lattice constants (a_0), bulk moduli (B_0) and cohesive energies (E_0). The cohesive energies were calculated as the differences of the bulk energies per atom and the isolated-atom energies. The counterpoise method [51] was applied to correct the basis set superposition error (BSSE) for the isolated atom, because atoms and molecules are much more sensitive to the basis set size than periodic systems. In estimating the BSSE, all atomic orbitals of nearest neighbours were taken into account (12 nearest neighbours for the fcc structure). As seen from table 1, the counterpoise error is quite large in our case, although the basis set is of double-zeta quality.

Table 1. Cohesive properties (lattice constant a_0, bulk modulus B_0, cohesive energy E_0) of the platinum bulk for different DFT functionals and the Hartree–Fock method. When calculating the cohesive energy, the counterpoise correction of the free platinum atom was taken into account (see the text). The basis set superposition error (BSSE) is specified in the last column for each method and is calculated as the difference between the energy of the free atom and the energy of the free atom with the counterpoise correction.

	a_0/Å	B_0/GPa Å^{-3}	E_0/eV	BSSE/eV
LDA/VWN	3.92	310	7.52	1.42
PBE	3.99	270	6.75	0.88
BPW91	3.99	270	5.67	0.75
BLYP	4.06	240	4.76	1.72
HF	4.04	175	0.36	1.14
Experiment	3.92[a]	278[b]	5.84[b]	

[a] Reference [52].
[b] Reference [53].

The lattice constant of 3.92 Å obtained with the LDA/VWN functional is practically the same as the experimental one [52], but all of the other functionals and the HF method give too-large constants. This LDA/VWN result is in contradiction with the usual LDA/VWN accepted wisdom (the functional usually gives too-short bond distances and too-large binding energies) and is probably due to the compensation of basis set errors. The experimental bulk modulus is estimated to be 278 GPa Å^{-3} [53], whereas the cohesive energy value is 5.84 eV [53]. The values of B_0 and the E_0 obtained using the BPW91 and PBE functionals are closest to the experimental ones. It is interesting that the BLYP functional, which has the same exchange functional as the BPW91 functional, gives a much larger lattice constant and lower bulk modulus and cohesive energy. This is entirely due to the different treatment of correlation in the PW91 and LYP functionals. The HF lattice constant is in between the BPW91 and BLYP constants, but the HF E_0 and B_0 are considerable underestimations. This is due to the neglect of correlation in the HF approximation. Figure 1 shows exchange and correlation energies as a function of the lattice constant for the functionals used and for an exact Fock exchange. It is seen that the exchange treatment of the LDA approximation is responsible for the lower a_0 and greater B_0 with respect to the GGA results, since its steep behaviour overcompensates for the lower slope of the VWN correlation energy.

In order to compare the results from the LCAO method as embodied in the CRYSTAL code with results obtained from some other accurate first-principles method, we have also performed some calculations for Pt bulk using the WIEN97 full-potential linearized-augmented-plane-wave (FP-LAPW) code [54]. Good agreement of the results from the two was obtained.

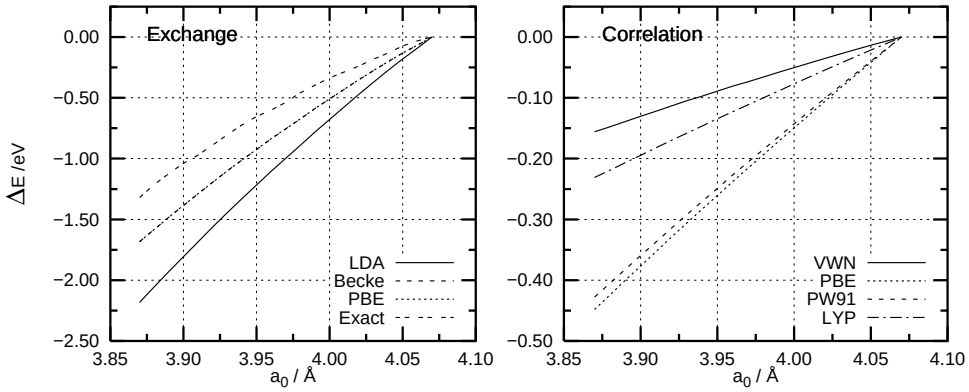

Figure 1. Exchange (left panel) and correlation (right panel) energies as functions of the lattice constant. The exact Fock exchange energy is shown as well. The Becke and PBE exchange curves almost coincide (they are seen as one curve). In order to compare different functionals, the last energy point of each functional is taken for individual zero levels.

WIEN97 yields a lattice constant of 3.98 Å and a bulk modulus of 260 GPa $Å^{-3}$ at the PBE level. The densities of states, band structures and electronic densities are quite similar as well.

3.2. Electronic structures

The electronic features of our bulk calculations were examined at the LDA/VWN level of theory by means of the band structure, the density of states and electron-density difference plots. The band structure and the density of states (DOS) presented in figure 2 are comparable with those computed by Elsässer *et al* [44] and MacDonald *et al* [43], respectively. The width of the d band, as seen from the DOS curve, is about 8 eV. The total DOS in the region shown is almost entirely due to d states, except for the s contribution at the bottom of the d band, which is in agreement with the study of Elsässer *et al* [44], and indicates the hybridization of the nearby empty s band (not shown in figure 2) with the valence d band. The contribution of the p states is low (almost an order of magnitude lower than that of the d states), but it is present through the entire d band.

Figure 3 shows a three-dimensional plot [55] of the electron-density difference between the bulk density and the corresponding superposition of the isolated-atom densities. The isosurface of zero difference is shown. There is a lack of electrons in the regions between the small star-like envelopes and the larger sphere-like envelopes. As a result, a transfer of electron density from the outer atom shells to the interstitial regions occurs, illustrating the effect of metallic chemical bonding. Elsässer *et al* [44] explained this feature in terms of s–d hybridization, although in our case the p contribution is not negligible as seen from the DOS curve in figure 2. The additional electronic charge around the cores (star-like envelopes) reduces the mutual electrostatic repulsions between the positively charged cores.

It is worth discussing and exploring the star-like shape of the inner envelope somewhat further. The envelope is oriented along the x-, y- and z-axes (E_g character), whereas the nearest-neighbour atoms are in all of the intermediate positions between the x-, y- and z-axes—that is, in the xy-, xz- and yz-positions (T_{2g} character). The star-like shape of the envelope indicates that the most occupied d orbitals should be the d_{z^2} and $d_{x^2-y^2}$ orbitals having the same occupancy, thus leaving the d_{xy}, d_{xz}, d_{yz} orbitals less occupied. This assumption is confirmed by Mulliken population analysis, which shows that the d_{z^2} and $d_{x^2-y^2}$ orbitals have

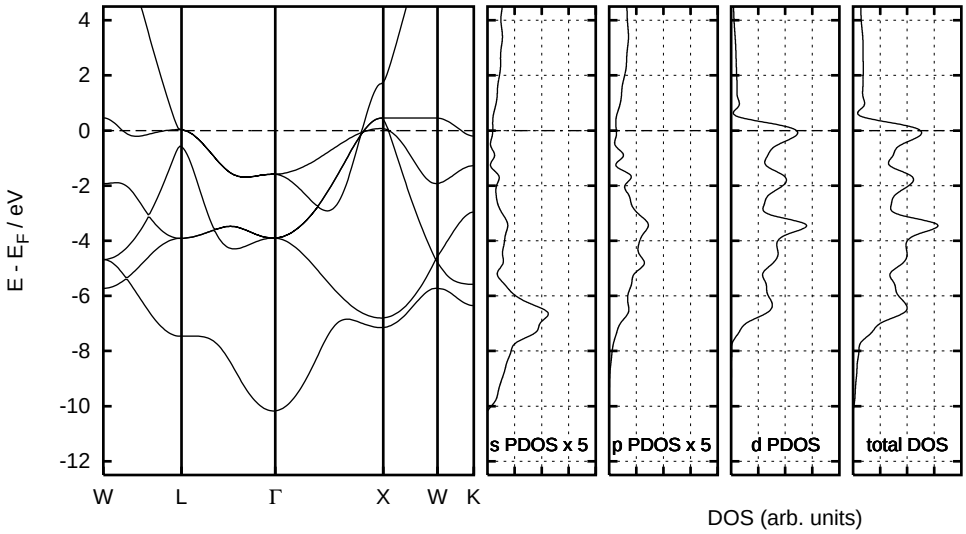

Figure 2. The LDA/VWN band structure, and the projected and total density of states (designated as the PDOS and total DOS, respectively). Going from the left to the right panels: band structure, density of states projected to s orbitals, to p orbitals, to d orbitals and the total DOS for the platinum bulk. The DOS projected to the s and p orbitals is magnified five times ($\times 5$).

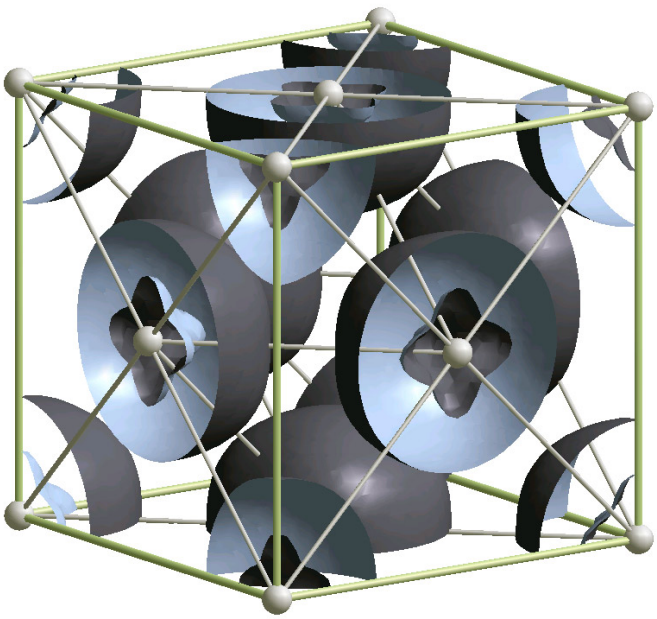

Figure 3. The LDA/VWN electron-density difference [55] between the bulk and the corresponding superposition of the atomic densities. The isosurface of zero difference is plotted, i.e. $\rho(\mathrm{Pt_{bulk}}) - \rho(\mathrm{Pt_{atom}}) = 0.0$. There is a lack of electrons in the regions between the small star-like envelopes and larger sphere-like envelopes.

0.146 electrons of additional charge with respect to the d_{xy}, d_{xz} and d_{yz} orbitals. This is not surprising since the larger nearest-neighbour interaction in the T_{2g} manifold pushes the antibonding T_{2g} states to higher energies than the antibonding E_g states. With a nearly full d band, this implies that more T_{2g} than E_g states are situated above the Fermi level.

4. Pt(111) slabs of different thicknesses

4.1. Surface energetics

Slabs consisting of one, two, three and four monolayers with (111) structures were considered, which were labelled from S1 to S4, in the following. Figure 4 displays the slab models where a few unit cells parallel to the slab directions are drawn. The inner layers of the S3 and the S4 slabs will be referred to as subsurface layers. In all cases the calculated equilibrium lattice constant was maintained as far as the two-dimensional layers are concerned (3.92 Å and 3.99 Å for the LDA/VWN and BPW91 functionals, respectively).

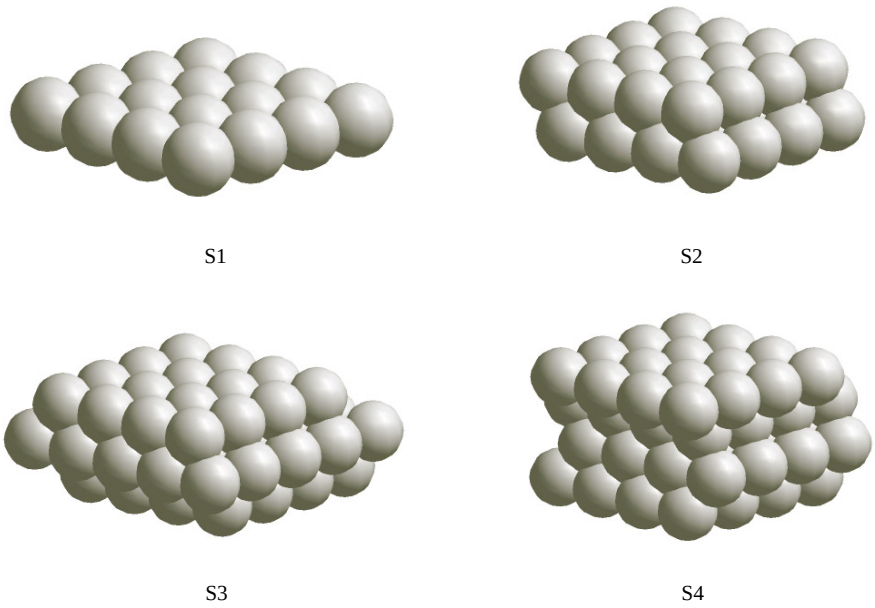

Figure 4. The slab models used in the study [55]. A few unit cells in the direction parallel to the slab are plotted.

Since the Pt(111) surface is known to be stable and exhibits no reconstruction, we need only search for relaxation of the surface layer without any reconstruction process. The relaxation distance (d_{relax}) designates the difference of the distance between (i) the surface and the subsurface layer for the relaxed slab and (ii) that for a non-relaxed slab in which interlayer distances were kept the same as in the crystal lattice. The relaxation energies (E_{relax}) were obtained as half the difference between the energy of the relaxed slab and that of the non-relaxed slab.

The surface energy per elementary cell (E_{surf}) was evaluated as

$$E_{surf}(n) = \frac{1}{2}[E_n - nE_b] \tag{1}$$

where E_n is the total energy per unit cell of an n-layer slab and E_b is the bulk total energy per unit cell. However, it is known that E_{surf} diverges as n increases [56]. Therefore we also calculated the surface energy by applying the equation proposed by Boettger for $n \leqslant N$, where N is the number of layers of the thickest slab employed [56, 57]:

$$E'_{surf}(n) = \frac{1}{2}[E_n - n\,\Delta E(N)]. \tag{2}$$

In this formula the bulk energy is approximated by the incremental energy $\Delta E(N)$:

$$\Delta E(N) = E_N - E_{N-1} \tag{3}$$

which is the difference between N-layer-slab and $(N-1)$-layer-slab total energies.

Relaxation distances, relaxation energies and surface energies are presented in table 2. From this table it is obvious that relaxation is negligible for Pt(111) surface energetics. The S2 and S4 slabs give the LDA/VWN relaxation distance as about 0.01 Å outward, whereas the S3 slab gives a relaxation distance of about 0.02 Å inward. The BPW91 relaxation distance for the S4 slab is about 0.02 Å outward. The experimental values of the relaxation distance range from 0 to 2% of the bulk planar spacing [7, 10–12, 58]. The recent study of Materer *et al* [8, 9] (using the LEED technique) estimated the relaxation distance of the surface layer to be 0.025 ± 0.01 Å outward, which is comparable with our relaxation distances for the S2 and S4 slabs. In contrast, the semi-empirical calculations using the equivalent-crystal theory (ECT) [20] and embedded-atom method (EAM) [17] predict an inward relaxation of up to 3% of the bulk planar spacing.

Table 2. Relaxation distances, relaxation energies and surface energies for the S1, S2, S3 and S4 slabs. The surface energy calculated with equation (1) is designated as E_{surf}, whereas the surface energy obtained from equation (2) for $N = 5$ is designated as E'_{surf}.

$\text{Slab}_{\text{method}}$	d_{relax}/Å	E_{relax}[a]/eV	E_{surf}/eV	E'_{surf}/eV	E'_{surf}[b]/erg cm^{-2}
$\text{S1}_{\text{LDA/VWN}}$	—	—	1.15	1.05	2530
$\text{S2}_{\text{LDA/VWN}}$	0.013	5.7×10^{-4}	1.27	1.07	2580
$\text{S3}_{\text{LDA/VWN}}$	−0.019	2.4×10^{-3}	1.39	1.09	2620
$\text{S4}_{\text{LDA/VWN}}$	0.012	1.6×10^{-3}	1.46	1.06	2550
S4_{BPW91}	0.017	2.1×10^{-3}	1.23	0.70	1630
Experiment	0.025[c]	—	—	—	2490[d]

[a] Relaxation energies are beyond the precision of our calculations, but are specified just to indicate how small these energies are.
[b] 1 erg $= 10^{-7}$ J.
[c] References [8, 9].
[d] Corresponds to an 'average' high-index surface. See reference [62].

Relaxation energies are beyond the precision of our calculations, but are specified in table 2 merely to indicate how small these energies are.

As seen from the same table, the surface energies calculated with equation (1) increase with slab thickness and the LDA/VWN value of 1.46 eV for the S4 slab is too large. The surface energies calculated with equation (2), where the bulk energy was approximated as the difference between the total energies of five- and four-layer slabs ($\Delta E(N = 5)$) are in better agreement with experiment. The surface energies, E'_{surf}, for the S4 slab are 1.06 and 0.70 eV for the LDA/VWN and BPW91 functionals, respectively. The fact that the GGA yields a lower surface energy can be explained following the relation proposed by Methfessel *et al* [61], which relates surface energy to 'non-magnetic' cohesive energy, E'_{coh}, where the

'non-magnetic' cohesive energy stands for the difference between the non-magnetic free-atom total energy and the bulk total energy. The relation is

$$E_{surf} = \frac{C_B^{1/2} - C_S^{1/2}}{C_B^{1/2}} E'_{coh} \tag{4}$$

where C_B is the coordination number in the bulk and C_S is the coordination number of a surface atom. This equation tells us that the LDA should yield greater surface energies than the GGA, since the LDA overestimates the bond strengths. For an fcc (111) surface the factor $(C_B^{1/2} - C_S^{1/2})/C_B^{1/2}$ is 0.134 ($C_B = 12$, $C_S = 9$). Thus the difference between LDA/VWN and BPW91 surface energies can be approximated as

$$\Delta E_{surf} = 0.134 \times [E'_{coh_{\mathrm{LDA/VWN}}} - E'_{coh_{\mathrm{BPW91}}}]. \tag{5}$$

The 'non-magnetic' cohesive energies are 8.42 and 6.80 eV for LDA/VWN and BPW91 functionals, respectively. Therefore, qualitatively speaking, the difference of 0.22 eV obtained from equation (5) is similar to our calculated values of ΔE_{surf} of 0.23 eV and 0.36 eV obtained from equations (1) and (2), respectively. The LDA/VWN surface energies seem to be too high, since the experimental surface energy obtained by Tyson and Miller [62] is 2490 erg cm^{-2} and corresponds to an 'average' high-index surface. As shown by Ning *et al* [17], Rodríguez *et al* [20] and Methfessel *et al* [61], the (111) surface has the lowest surface energy per unit area among the series of calculated values for different crystalline faces. It is questionable, but tempting, to discuss the accuracy of LDA and GGA surface energies on the basis of equation (4). Since the BPW91 approximation yields a better cohesive energy than the LDA/VWN (see table 1), one may conclude from equation (4) that it should yield a better surface energy as well. The BPW91 value of 1630 erg cm^{-2} obtained from equation (2) seems low, but Rodríguez *et al* [20] calculated, by means of equivalent-crystal theory (ECT), the Pt(111) surface energy to be 1716 erg cm^{-2}, whereas the surface energies for (001), (110) and most high-index surfaces range from 2000 to 2700 erg cm^{-2}.

As a consequence of the fact that relaxation has such a small impact on the surface energetics, it can be expected that neglecting the relaxation will not affect the surface properties calculated with our model. Relaxation does not have any influence on the two-dimensional average electrostatic potential above the surface (the influence of the relaxation is of the order of 10^{-4} au). The two-dimensional average electrostatic potential is defined as

$$\overline{V}(z) = \frac{1}{a}\int_a V(x, y, z)\,\mathrm{d}x\,\mathrm{d}y. \tag{6}$$

Even the S1 slab, whose relaxation cannot be accounted for, has a very similar two-dimensional average electrostatic potential above the surface. This is shown in figure 5. On the basis of these data, one can conclude that only the first layer is actually effective, since contributions from inner layers are rapidly quenched.

Any possible local change in the electron-density distribution, which may play an important role in the adsorbate/substrate interaction, should be investigated to exploit the slab model employed even further.

4.2. Electronic properties of slabs

The electronic properties of slabs can be discussed considering the reduced coordination number of surface atoms. This reduction results in a redistribution of the charge between and within the s, p and d bands, and in the narrower, more atomic-like d bands with a reduced s–d hybridization [63]. The surface atoms of the late transition metals and noble metals are expected to have a greater fraction of the electron charge arising from d states than the

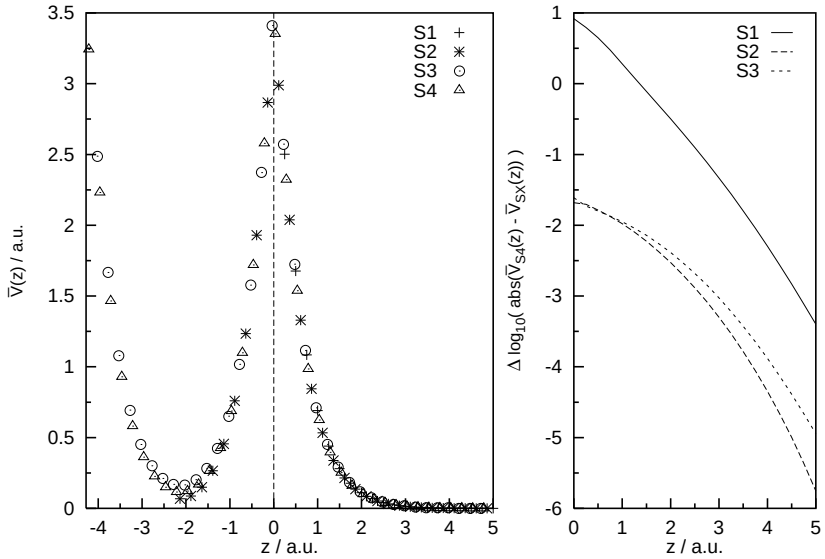

Figure 5. The LDA/VWN average electrostatic potential, equation (6), along the slab normal. The surface layer is at the position $z = 0$, whereas the subsurface layer is at the position of the ordinate axis. Left: the potential is plotted in the region above the surface ($z > 0$) for all slab models. In addition, the region contained between the surface and subsurface layer is plotted for the S3 and S4 slabs as well. The additional region for the S2 slab extends from $z = 0$ to the middle of the slab. Right: the base-10 logarithm of the potential difference (in au) for the S1, S2 and S3 slabs ($\overline{V}_{SX}(z)$, $X = 1, 2, 3$) with respect to the S4 slab in the region above the surface ($z > 0$).

corresponding bulk atoms. These effects are manifested in surface-atom core-level shifts (SCSs) [63, 64, 68]. For transition metals with less-than-half-filled d bands, the surface-atom core levels are shifted to higher binding energies; the opposite is true for metals with more-than-half-full d bands. Dückers *et al* [69] measured the SCS of Pt(111) surface atoms with the Y Mζ radiation of the 4f spectra and estimated it to be -0.37 eV. Since the 4f states are contained in the RECP in our calculations, the lowest state was the 5s one. The calculated SCSs for that state are -0.385 and -0.392 eV for the S3 and S4 slabs, respectively. When comparing these SCSs to the experimental value, two things should be kept in mind:

(i) Our SCSs are the so-called 'initial-state' SCSs, also known as the core-eigenvalue shifts [65]. Alden *et al* have shown [66] that the core-eigenvalue shifts are indeed similar to the experimentally observed SCSs, although the former quantity might have no direct relevance for the latter. Their 'final-state' SCS for the 4f level was calculated to be -0.423 eV.

(ii) Methfessel *et al* [67] have shown that SCSs are very similar for all core states of an atom for the late transition metals.

A straightforward approach for exploring changes of surface-atom orbital population with respect to that of the bulk atom is Mulliken population analysis. But its results should be treated with caution, since the analysis is basis set dependent. However, it can give some qualitative insight, particularly when similar systems calculated with the same basis set are compared. A comparison of the orbital population of the surface atom with respect to that of the bulk atom reveals the expected increase of the population of surface d states and the decrease of the population of surface sp states. There is also a charge transfer within the d states. While

in the bulk the d states are populated according to fcc E_g and T_{2g} symmetry, the surface-atom d states are populated in a hcp manner; that is, the order of the d-orbital occupancy for the S3 and S4 slabs is $d_{z^2} > d_{x^2-y^2} = d_{xy} > d_{xz} = d_{yz}$.

The S4 slab gives a bulk–bulk bond population of 0.118 au, which is very close to the value of 0.117 au obtained from the bulk calculation. The population of the surface–surface bond is higher and equals 0.154 au. This is due to the reduced coordination number of surface atoms.

Some interesting features, however, are noticed when considering the atomic dipole and quadrupole moments along the direction perpendicular to the surface of the slab, as summarized in table 3. These quantities can be used as a measure of the electron cloud's deformation on the surface with respect to the isotropic situation existing in the bulk. In the bulk the first multipole moment different from zero is the $l = 4, m = 0$ contribution. The S3 slab shows some anomalies because its dipole moment is positive and about one hundred times smaller in magnitude than the dipole moment of the S2 slab. This indicates a very small displacement of the electron charge towards the interior of the slab. Such an anomaly in the dipole moments can explain why the relaxation distance is positive for the S2 and S4 slabs and negative for the S3 slab. For the S2 and S4 slabs the outward charge transfer increases the Coulombic repulsive attraction of the positively charged cores which causes an outward relaxation. Because the charge transfer is greater in the S2 case, its relaxation is greater as well (although very small). The inward charge transfer of the S3 slab causes just the opposite effect—that is, a better screening of the repulsive Coulombic attraction of the positively charged cores. This can be verified by observing the dipole moment changes when the relaxation distance is further decreased by artificially bringing the surface layer near to the subsurface layer. This approach causes an increase of the dipole moment D_z, indicating a further displacement of the electron charge towards the interior of the slab. That is, at shorter nucleus–nucleus distances the Coulombic repulsive attraction increases and the electron cloud tends to decrease this repulsion by displacing itself among the positively charged cores. Also the subsurface layer of the S3 slab must compensate for the charge transfer from both surface layers, which makes it additionally negative, resulting in better nucleus–nucleus screening. So we believe that this explains the anomaly of the relaxation of the S3 slab.

Table 3. Dipole (D_z) and quadrupole (Q_z) moments of the surface atom and subsurface atom for slabs with different numbers of layers (in 10^{-3} au). D_z and Q_z belong to a component perpendicular to the slab (Q_z is the $2z^2 - x^2 - y^2$ component of the quadrupole moment).

	Atom	S1	S2	S3	S4
D_z	Surface	0.0	−288	2.36	−117
	Subsurface	—	—	0.0	194
Q_z	Surface	−1656	−1074	−1279	−1210
	Subsurface	—	—	241	103

The values for the quadrupole component perpendicular to the slab show no anomalies. Their negative values indicate an elongation undergone by the electron cloud of the surface atoms. Sublayer atoms of the S3 and S4 slabs show the squeezing of their electron clouds, indicating that the first sublayer is not a good bulk layer yet.

In figure 6 the three-dimensional electron-density difference between the electron density of the slab and the corresponding superposition of the free-atomic densities is presented for all slab models. The isosurface of zero difference is plotted for a few unit cells in a direction parallel to the slab. It is easily seen from that figure that the electron-density difference for the S1 slab

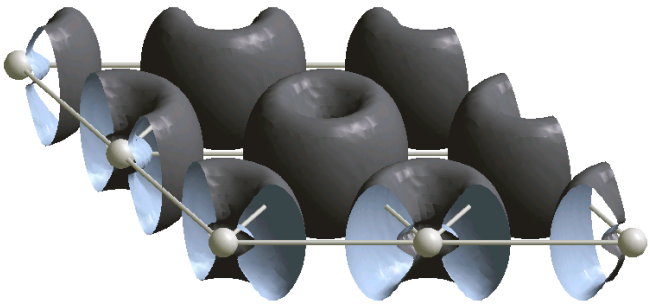

(a)

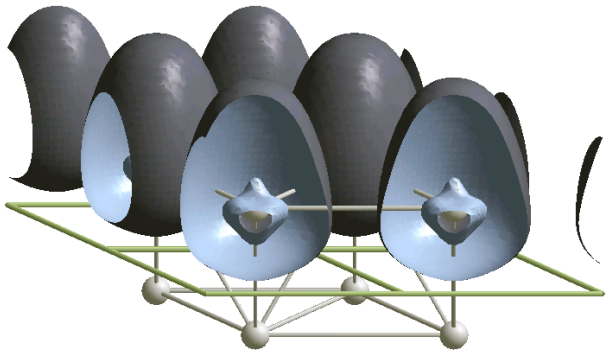

(b)

Figure 6. The LDA/VWN electron-density differences [55] between the densities of various slab models and the corresponding superposition of atomic densities—(a), (b), (c), (d) correspond to the S1, S2, S3 and S4 slabs, respectively. The isosurface of the zero difference is plotted, i.e. $\rho(\mathrm{Pt_{slab}}) - \rho(\mathrm{Pt_{atom}}) = 0.0$. Two unit cells in both crystallographic directions parallel to the (111) surface are drawn as indicated by the unit-cell borders in the middle of the S2 and S4 slabs. The electron-density differences are cut along the unit-cell boundaries. For the S1 slab the region contained inside the torus-like closed isosurface suffers a lack of electrons. For the S2, S3 and S4 slabs the lack of electrons for the surface layer is in the region between the spinning-top-shaped and egg-shaped isosurfaces, whereas for the subsurface layers of the S3 and S4 slabs the lack of electrons is between the smaller and larger closed isosurfaces. The electron-density difference is shown only on the upper side of the S2, S3 and S4 slab models to enhance the readability of the plots.

totally differs from those of the S2, S3 and S4 slabs. For the S1 slab the region contained inside the torus-like closed surface suffers a lack of electrons, whereas the interstitial regions have an excess of electrons. The hole inside the 'torus' has the shape of the d_{z^2} orbital, which is not surprising because of the great d_{z^2} occupancy as revealed from Mulliken population analysis. For the S2, S3 and S4 slabs the lack of electrons for the surface layer is in the region between the smaller spinning-top-shaped isosurface and the larger egg-shaped isosurface, whereas for the subsurface layers of the S3 and S4 slabs the lack of electrons is between the smaller and larger closed isosurfaces.

The band structure and the density of states (DOS) of the S4 slab and the (111)-projected bulk band structure are shown in figure 7. The first impression is of a good correspondence of the (111)-projected bulk band structures with those of the slab. The projected bulk Pt(111)

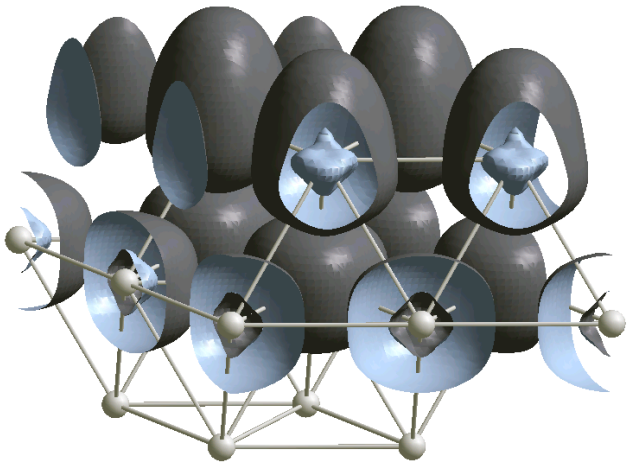

(c)

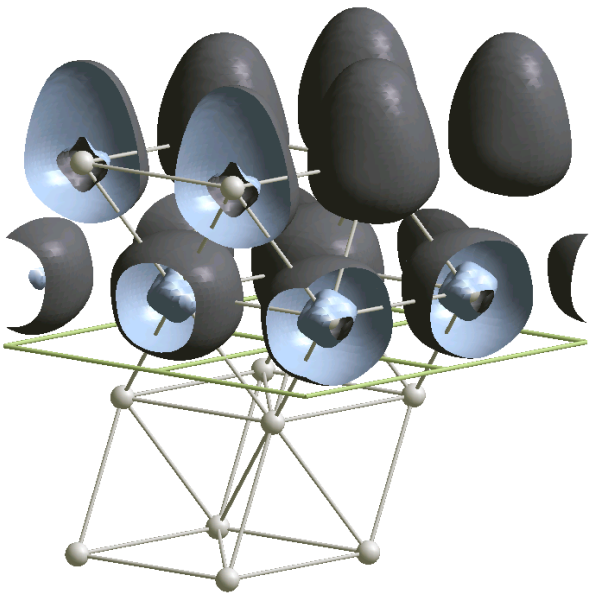

(d)

Figure 6. (Continued)

band structure is very similar to the band structure obtained, for example, by Tapilin *et al* [5] with the LMTO-TB method. Only one surface state can be recognized with certainty from visual examination of the plots (marked with a bold line). As mentioned in reference [60], the fact that the position of the surface states does not change with increasing slab thickness is a good indicator that the slab is thick enough to represent a reliable model of the selected crystalline face. The recognized surface state exhibits only minor changes from the S2 to the S4 slab (not shown), indicating that even the S2 slab may be appropriate as a relevant model of the (111) crystalline face. The DOS of the slab is more jagged than the bulk DOS, and thus

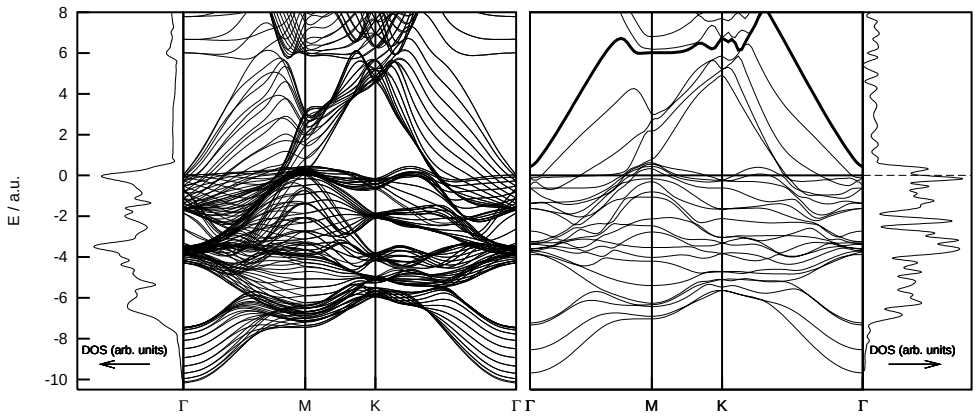

Figure 7. LDA/VWN band structures (BAND) with the corresponding densities of states (DOS). Left: the DOS and the (111)-projected BAND for the bulk. Right: the BAND and DOS for the S4 slab. Only one surface state is recognized (marked with the bold line). The Fermi energy of the S4 slab is set as the zero level.

a comparison is difficult. The peaks are narrower and sharper. Figure 8 shows DOS curves projected to the surface and subsurface layer for the S4 slab and a comparison with the bulk DOS is made. The integrated-density-of-states (IDOS) comparison shows good matching of the S4 subsurface layer's IDOS and the IDOS of the bulk atom. Even for the S3 slab the matching between the subsurface layer's IDOS and the corresponding bulk calculation IDOS is good (not shown).

5. Conclusions

Bulk platinum and platinum slabs one to four (111) layers thick have been studied by means of the HF and DFT CO–LCAO CRYSTAL program. First the bulk was considered, because it is difficult to believe that an approach which gives an inadequate description of the bulk could treat the surface successfully. The calculated properties of the bulk seem to be reasonable when comparing them with experimental values. The results of the bulk calculations may be summarized as follows:

(i) The lattice constants calculated with different functionals show a small overestimation (0.00, 0.07, 0.07, 0.14 Å for the LDA/VWN, BPW91, PBE, BLYP functionals, respectively). The same calculations provide bulk moduli and cohesive energies that fall around the experimental values (the LDA/VWN functional overestimates, the BLYP functional underestimates, whereas the BPW91 and PBE functionals give almost the experimental bulk modulus). The basis set superposition corrections are significant for the free-atom total energies and care should be taken when estimating the cohesive energies. Correlation effects are important, as is evident from comparison of the DFT and HF results.

(ii) The band structure, density of states and width of the d band (8 eV) obtained from the LDA/VWN density-of-states curve are comparable with those obtained from the literature. At the bottom of the d band some contribution from s states is observed, whereas a small p-state contribution is present throughout the entire d band. The s and p contributions arise from the nearby s and p bands.

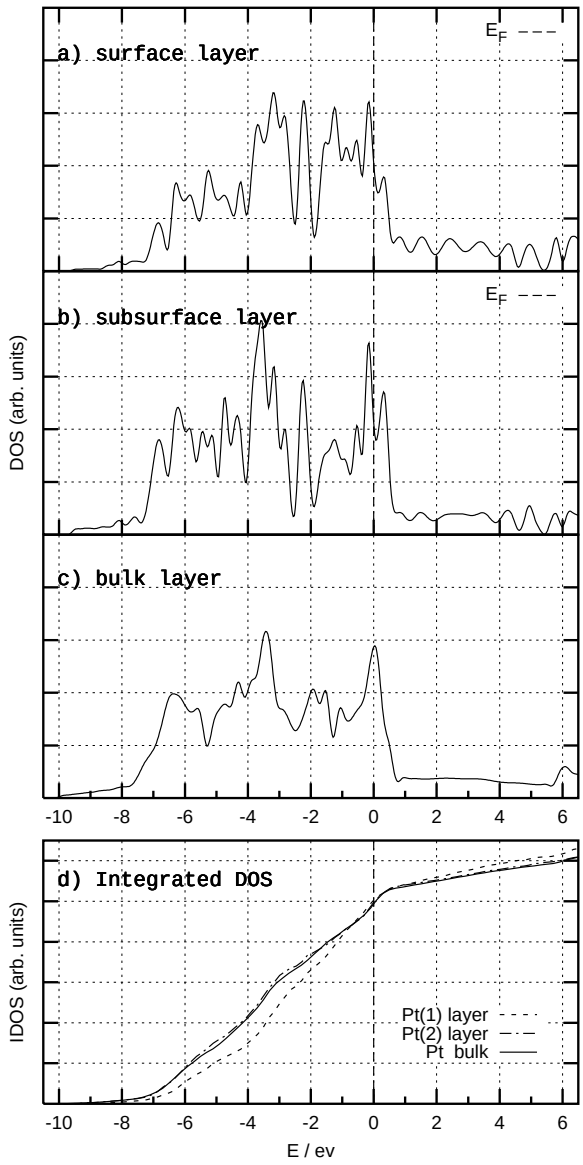

Figure 8. The LDA/VWN density of states projected to: (a) the surface, (b) the subsurface (slab's bulk) layer for the S4 slab; and (c) the density of states obtained by the bulk calculation. The bottom panel (d) shows a comparison of the integrated density of states for cases (a), (b), (c). The Fermi energy is set as the zero level (vertical dashed line).

A detailed investigation of the Pt(111) slabs provides evidence that various features show a different dependence on slab thickness. Some important results concerning the Pt(111) slabs are as follows:

(i) The relaxation exhibits an anomaly for the S3 slab, which produces a negative LDA/VWN relaxation distance of -0.02 Å. The relaxation distance of the S4 slab is 0.01 Å and 0.02 Å for the LDA/VWN and BPW91 functionals, respectively, and is compatible with the experimental data. The dipole moment component perpendicular to the slab exhibits an anomaly for the S3 slab as well. We believe that these two anomalies are closely related. The relaxation energies are of the order of 10^{-3} eV. It is clear that these small relaxation distances and energies are of minor importance, thus leading to the conclusion that relaxation effects can be neglected when modelling the Pt(111) surface. The calculated surface energies are 1.06 and 0.70 eV for LDA/VWN and BPW91 functionals, respectively.

(ii) The quadrupole moment components perpendicular to the slab show an elongation of the surface atom's electron cloud for all slab models and a squeezing of the sublayer atom's electron cloud for the S3 and S4 slabs. This picture from the quadrupole moment analysis is confirmed by the electron-density difference plots.

(iii) The band structures of the slab models studied are very similar and show a good correspondence to the (111)-projected bulk band structure.

(iv) The density of states seems to be the feature most dependent on slab thickness among all the properties investigated. Density-of-states curves, electron-density difference maps and Mulliken orbital population analysis reveal that the first sublayer is not yet a good bulk layer.

The S4 slab was found to be adequate as a model of the Pt(111) surface. There are also some indications that even S3 might be used as a model of the surface, but the anomaly of the relaxation distance and dipole moment of the surface layer for the S3 slab raised doubts about that. To find out the effect of this anomaly on adsorption properties, further investigations of slab models were carried out and will be published elsewhere [70].

Acknowledgments

Financial support of this work was provided by the Ministry of Science and Technology of Slovenia, Grant No J1-7339. The authors would like to thank A Lesar, I Kobal, M Hodošček, P W M Jacobs and Y F Zhukovskii for reading the manuscript and for helpful discussions.

References

[1] Taylor K C 1993 *Catal. Rev. Sci. Eng.* **35** 457
[2] Shelef M and Graham G W 1994 *Catal. Rev. Sci. Eng.* **36** 443
[3] Zhdanov V P and Kasemo B 1997 *Surf. Sci. Rep.* **29** 31
[4] Somorjai G A 1994 *Introduction to Surface Chemistry and Catalysis* (New York: Wiley) ch 7
[5] Tapilin V M, Zemlyanov D Y, Smirnov M Y and Gorodetskii V V 1994 *Surf. Sci.* **310** 155
[6] Kesmodel L L, Stair C P and Somorjai G A 1977 *Surf. Sci.* **63** 342
[7] Adams D L, Nielsen H B and Van Hove M A 1979 *Phys. Rev.* B **20** 4789
[8] Materer N, Barbieri A, Gardin D, Starke U, Batteas J D, Van Hove M A and Somorjai G A 1994 *Surf. Sci.* **303** 319
[9] Materer N, Starke U, Barbieri A, Döll R, Heinz K, Van Hove M A and Somorjai G A 1995 *Surf. Sci.* **325** 207
[10] Bogh E and Stensgaard I 1978 *Phys. Lett.* A **65** 357
[11] Davies J A, Jackson D P, Norton P R, Posner D E and Unertl W N 1980 *Solid State Commun.* **34** 41
[12] van der Veen J F, Smeenk R C, Tromp R M and Saris F W 1979 *Surf. Sci.* **79** 219
[13] Chan A W E, Hoffmann R and Ho W 1992 *Langmuir* **8** 1111
[14] Tamura E and Feder R 1989 *Solid State Commun.* **70** 205
[15] Benesh G A, Liyanage L S and Pinglet J C 1990 *J. Phys.: Condens. Matter* **2** 9065
[16] Tsai M H and Hass K C 1995 *Phys. Rev.* B **51** 14 616

[17] Ning T, Yu Q and Ye Y 1988 *Surf. Sci.* **206** L857
[18] Majerus J, Castellani N J and Légaré P 1994 *Surf. Sci.* **311** L661
[19] Smith J R, Perry T, Banerjea A, Ferrante J and Bozzolo G 1991 *Phys. Rev.* B **44** 6444
[20] Rodríguez A M, Bozzolo G and Ferrante J 1993 *Surf. Sci.* **289** 100
[21] Needs R J, Godfrey M J and Mansfield M 1991 *Surf. Sci.* **242** 215
[22] Feibelman P J 1997 *Phys. Rev.* B **56** 2175
[23] Dovesi R, Saunders V R, Roetti C, Causà M, Harrison N M, Orlando R and Aprà E 1996 *CRYSTAL95—User's Manual* University of Torino
[24] Stevens W J, Krauss M, Bash H and Jansien P G 1992 *Can. J. Chem.* **70** 612
[25] The results obtained using the RECP of Stevens *et al* [24] without the f-projection term were not published, but the calculations were performed in conjunction with our previous cluster study:
Kokalj A, Lesar A and Hodošček M 1997 *Chem. Phys. Lett.* **268** 43
[26] Feibelman P J 1995 *Phys. Rev.* B **51** 17 687
[27] Feibelman P J, Esch S and Michely T 1996 *Phys. Rev. Lett.* **77** 2257
[28] Feibelman P J 1997 *Phys. Rev.* B **56** 10 532
[29] Dovesi R, Pisani C, Ricca F and Roetti C 1982 *Phys. Rev.* B **25** 3731
[30] Dovesi R, Ferrero E, Pisani C and Roetti C 1983 *Z. Phys.* B **51** 195
[31] Dovesi R, Pisani C and Roetti C 1983 *Gazz. Chim. It.* **113** 313
[32] Moruzzi V L, Janak J F and Williams A R 1978 *Calculated Electronic Properties of Metals* (New York: Pergamon) p 13
[33] Pulay P 1980 *Chem. Phys. Lett.* **73** 393
[34] Monkhorst H J and Pack J D 1976 *Phys. Rev.* B **13** 5188
[35] Gilat G and Raubenheimer L J 1996 *Phys. Rev.* **144** 390
[36] Dirac P A M 1930 *Proc. Camb. Phil. Soc.* **26** 376
[37] Vosko S H, Wilk L and Nusair M 1980 *Can. J. Phys.* **58** 1200
[38] Becke A D 1988 *Phys. Rev.* A **38** 3098
[39] Perdew J P and Wang Y 1986 *Phys. Rev.* B **33** 8800
Perdew J P and Wang Y 1989 *Phys. Rev.* B **40** 3399
Perdew J P and Wang Y 1992 *Phys. Rev.* B **45** 13 244
[40] Causà M and Zupan A 1994 *Chem. Phys. Lett.* **220** 145
[41] Andersen O K 1970 *Phys. Rev.* B **4** 883
[42] Smith N V 1974 *Phys. Rev.* B **9** 1365
[43] MacDonald A H, Damms J M, Vosko S H and Koelling D D 1981 *Phys. Rev.* B **23** 6377
[44] Elsässer C, Takeuchi N, Ho K M, Chan C T, Braun P and Fähnle M 1990 *J. Phys.: Condens. Matter* **2** 4371
[45] See references in:
Ahuja R, Solanki A K and Auluck S 1991 *Phys. Status Solidi* b **168** 509
[46] See for example reference [50] and references cited in reference [64].
[47] Lee C, Yang W and Parr R G 1988 *Phys. Rev.* B **37** 785
[48] Perdew J P, Burke K and Ernzerhof M 1996 *Phys. Rev. Lett.* **77** 3865
Perdew J P, Burke K and Ernzerhof M 1997 *Phys. Rev. Lett.* **78** 1396
[49] Roothaan C C J 1960 *Rev. Mod. Phys.* **32** 179
[50] Aschroft N W and Mermin N D 1976 *Solid State Physics* (Philadelphia, PA: Saunders)
[51] Boys S F and Bernardi F 1970 *Mol. Phys.* **19** 553
[52] Wyckoff R W G 1963 *Crystal Structures* 2nd edn (New York: Interscience)
[53] Kittel C 1986 *Introduction to Solid State Theory* 6th edn (New York: Wiley) pp 55–7
[54] Blaha P, Schwarz K and Luitz J 1999 *A Full Potential Linearized Augmented Plane Wave Package for Calculating Crystal Properties* Karlheinz Schwarz, Technical University of Vienna (ISBN 3-9501031-0-4)
This is an improved and updated Unix version of the original copyrighted WIEN code, which was published by Blaha P, Schwarz K, Sorantin P and Trickey S B 1990 *Comput. Phys. Commun.* **59** 399
[55] The three-dimensional plots in this paper were produced by the XCrySDen graphical package;
Kokalj A 1999 *J. Mol. Graphics Modell.* submitted
Kokalj A and Causà M 1999 *J. Comput.-Aided Mol. Design* submitted
[56] Boettger J C 1994 *Phys. Rev.* B **49** 16 798
[57] Boettger J C, Birkenheuer, Rösch N and Trickey S B 1994 *Int. J. Quantum Chem.: Quantum Chem. Symp.* **28** 675
[58] Ogletree D F, Van Hove M A and Somorjai G A 1986 *Surf. Sci.* **173** 351
[59] Loffreda D, Simon D and Sautet P 1998 *J. Chem. Phys.* **108** 6447
[60] Pisani C 1996 *Quantum-Mechanical ab initio Calculation of the Properties of Crystalline Materials* ed C Pisani

(Berlin: Springer) ch 13, pp 227–44
[61] Methfessel M, Hennig D and Scheffler M 1992 *Phys. Rev.* B **46** 4816
[62] Tyson W R and Miller W A 1997 *Surf. Sci.* **62** 267
[63] Citrin P H and Wertheim G K 1982 *Phys. Rev.* B **27** 3176
[64] Beatzold R C 1990 *Theoretical Aspects of Heterogeneous Catalysis* ed J B Moffat (Princeton, NJ: Van Nostrand-Reinhold) ch 11, pp 458–505
[65] Alden M, Skriver H L and Johansson B 1993 *Phys. Rev. Lett.* **71** 2449
[66] Alden M, Abrikosov A I, Johansson B, Rosengaard N M and Skriver H L 1994 *Phys. Rev.* B **50** 5131
[67] Methfessel M, Hennig D and Scheffler M 1993 *Surf. Sci.* **287/288** 785
[68] Desjonquères M C, Spanjaard D, Lassailly Y and Guilliot C 1980 *Solid State Commun.* **34** 807
[69] Dückers K, Bonzel H P and Wesner D A 1986 *Surf. Sci.* **166** 141
[70] Kokalj A, Lesar A, Hodošček M and Causà M 1999 *J. Phys. Chem.* B **103** 7222